Species separation and kinetic effects in collisional plasma shocksa)

C. Bellei, H. Rinderknecht, A. Zylstra, M. Rosenberg, H. Sio, C. K. Li, R. Petrasso, S. C. Wilks, and P. A. Amendt

Citation: Physics of Plasmas (1994-present) **21**, 056310 (2014); doi: 10.1063/1.4876614
View online: http://dx.doi.org/10.1063/1.4876614
View Table of Contents: http://scitation.aip.org/content/aip/journal/pop/21/5?ver=pdfcov
Published by the AIP Publishing

Species separation and kinetic effects in collisional plasma shocks[a)]

C. Bellei,[1,b),c)] H. Rinderknecht,[2] A. Zylstra,[2] M. Rosenberg,[2] H. Sio,[2] C. K. Li,[2] R. Petrasso,[2] S. C. Wilks,[1] and P. A. Amendt[1]
[1]*Lawrence Livermore National Laboratory, 7000 East Avenue, Livermore, California 94550, USA*
[2]*Plasma Science and Fusion Center, Massachusetts Institute of Technology, Cambridge, Massachusetts 02139, USA*

(Received 14 December 2013; accepted 2 April 2014; published online 19 May 2014)

The properties of collisional shock waves propagating in uniform plasmas are studied with ion-kinetic calculations, in both slab and spherical geometry and for the case of one and two ion species. Despite the presence of an electric field at the shock front—and in contrast to the case where an interface is initially present [C. Bellei *et al.*, Phys. Plasmas **20**, 044702 (2013)]—essentially no ion reflection at the shock front is observed due to collisions, with a probability of reflection $\lesssim 10^{-4}$ for the cases presented. A kinetic two-ion-species spherical convergent shock is studied in detail and compared against an average-species calculation, confirming effects of species separation and differential heating of the ion species at the shock front. The effect of different ion temperatures on the DT and D^{3}He fusion reactivity is discussed in the fluid limit and is estimated to be moderately important. © *2014 AIP Publishing LLC*. [http://dx.doi.org/10.1063/1.4876614]

I. INTRODUCTION

Current state-of-the-art simulation codes that are used to design inertial confinement fusion (ICF) experiments on the National Ignition Facility (NIF) and on the OMEGA facility assume that the dynamics of an ICF implosion can be well described by a fluid approximation with a single momentum equation for the average-ion species and neglecting electric and magnetic fields.

For a system that is entirely dominated by collisions (fluid limit), the effects of species diffusion, electric fields, and kinetic effects (departure from a Maxwellian distribution function) are certainly negligible. However, several experiments have already shown signatures of this "missing" physics: from the presence of electric fields during ICF implosions,[1,2] to anomalies in the fusion yield in mixtures of D_2 and ^{3}He gas[3] and in DT gas.[4] More recently, standard hydrodynamic codes have been challenged by experiments designed to test the codes in the limits of large mean-free-paths.[5,6] From a theoretical and simulation point of view, there is also evidence that more detailed numerical models may be necessary in order to correctly interpret many ICF experiments.[7–9]

However, so far these efforts have not clearly identified serious consequences of non-fluid effects in ignition experiments, establishing that the core physics descriptions in current ICF codes is essentially intact and captures the key aspects of an ICF implosion.

Nevertheless, a demonstration of ignition is eagerly awaited, and prudence dictates understanding these regimes of physics in detail. In particular, these effects may erode ignition margins at the 1.5 MJ scale to complicate the path to an ignition demonstration. Moreover, for ICF to be an economically viable source of energy, our uncertainties on the outcome of ICF experiments must be reduced as much as possible, i.e., our understanding of the underlying physics must improve considerably. This leaves room for studies of basic physics, such as described in this paper, in the hope of improving significantly the accuracy of our predictions.

The aim of this paper is to study two aspects that are neglected in standard ICF codes. One aspect is that in a plasma, shocks have an electric field associated with the shock front and the ion distribution function may be non-Maxwellian near the shock front. The other aspect is that for mixtures of two or more distinct ion species, the dynamics may not be well described by a single average-ion species approach. While this work will show that significant ion reflection at the shock front is excluded, at least for ICF conditions and away from material interfaces, it will also confirm (through kinetic calculations) the possibility of significant species separation during the convergence of spherical shocks in low density gas fills.

This paper is structured as follows. Section II presents a series of ion kinetic simulations for a shock propagating in a uniform plasma and describes the dependence of the shock width and electrostatic potential as a function of Mach number. In Sec. III, spherical simulations relevant to ICF implosions are presented, with the intent of comparing an average-species description against a two-species one. Since these simulations predict that, in general, different ion species can have different temperatures on ICF timescales, in Sec. IV, we discuss how this can affect the fusion yield.

II. KINETIC SHOCKS IN A UNIFORM PLASMA AND SLAB GEOMETRY

Since the work of Jukes and Shafranov,[10,11] it is clear that shocks traveling in a collisional plasma maintain a self-consistent electric field at the shock front. In a single component plasma, the magnitude of the electrostatic potential jump across the shock front can be estimated as[12,13]

[a)]Paper GI3 6, Bull. Am. Phys. Soc. **58**, 106 (2013).
[b)]Invited speaker.
[c)]bellei1@llnl.gov

$$\Delta\Phi \approx k_B T_2 \ln(\rho_2/\rho_1)/e\,, \tag{1}$$

where k_B is Boltzmann's constant, T_2 is the temperature behind the shock, e the electron charge and ρ_2 (ρ_1) is the density of the shocked (unshocked) plasma. In what follows, we will refer to the approximation given by Eq. (1) as $\Delta\Phi^*$, i.e., $\Delta\Phi^* := k_B T_2 \ln(\rho_2/\rho_1)/e$.

The presence of an electric field is certainly important in collisionless plasmas, where one of the clear signatures is the reflection of ions at the shock front.[14] The aim of this section is to answer the question whether or not electric fields can significantly affect the structure of a collisional plasma shock that travels in a uniform plasma. The answer is, as it will shown shortly, negative.

One way of showing this is to write the fluid equations for a plasma in steady state, which are appropriate to the case of a shock wave propagating in a uniform plasma, in slab geometry. After neglecting the electron momentum flux due to $m_e \ll m_i$ and the electron viscosity, the one-dimensional plasma momentum equation for a single ion component plasma reads

$$m_i n_i u_i \frac{\mathrm{d}u_i}{\mathrm{d}x} + \frac{\mathrm{d}}{\mathrm{d}x}(p_e + p_i) - \frac{\mathrm{d}}{\mathrm{d}x}\left(\mu_i \frac{\mathrm{d}u_i}{\mathrm{d}x}\right) = (Zn_i - n_e)eE\,, \tag{2}$$

where n_i, m_i, and u_i are, respectively, the ion number density, mass and velocity; p_e and p_i are the electron and ion pressures, μ_i is the ion viscosity; Z is the ionization state of the ion and, finally, the electric field is denoted by the variable E.

After introducing the Debye length, λ_D, and the ion-ion mean free path, λ_{ii}, it can be shown that the term $(Zn_i - n_e)eE$ can be neglected in Eq. (2), since after writing $E = -\nabla p_e/en_e$ and using Gauss' law, one can estimate that at the shock front $(Zn_i - n_e)/n_e \sim (\lambda_D/\lambda_{ii})^2 \ll 1$. The equations describing the various thermodynamic variables in the problem (electron and ion velocity, temperature, density) are then decoupled from Poisson's equation.[15] In other words, in the limit of small Debye length $\lambda_D \ll \lambda_{ii}$, which is typically a very good approximation for ICF, the plasma equations for a steady shock coincide with the hydrodynamic equations for a fluid. Hence in this scenario, the bulk plasma is not affected by the presence of an electric field because of quasi-neutrality.

At the next level of detail we can ask whether or not at least part of the ion distribution function is affected by the electric field. As a first step, from the knowledge of the potential jump $\Delta\Phi$, the fraction of reflected ions φ_R can be easily calculated assuming that collisions are negligible. The quantity φ_R is the number of upstream ions with kinetic energy that, in the shock frame, is smaller than the electrostatic potential energy jump, over the total number of upstream ions

$$\varphi_R = \frac{\int_0^{\sqrt{2Ze\Delta\Phi/m_i}} f(v)\mathrm{d}v}{\int_{-\infty}^{+\infty} f(v)\mathrm{d}v}, \tag{3}$$

where $f(v)$ is the distribution function of the upstream ions in the shock frame. Next, we assume that $f(v)$ is given by a shifted Maxwellian distribution function, $f(v) \sim \exp[-(v - v_{sh})^2/2v_{th,1}^2]$, with v_{sh} being the shock velocity in the lab frame and $v_{th,1} = (k_B T_1/m_i)^{1/2}$ the thermal velocity in the upstream region. Note that the denominator in Eq. (3) counts all the ions in the upstream region, including those directed away from the shock; however, the latter population of ions only represents a small portion of the total upstream population, so that φ_R is only weakly dependent on whether or not these ions are included in the normalizing function.

The resulting fraction of reflected ions φ_R can then be plotted as a function of Mach number, as shown in Fig. 1 for the case $Z = 1$. As usual, Mach number is defined as the ratio of the shock speed over the upstream sound speed, $M = u_s/a_1$. The curves are parametrized with $\Delta\Phi = \Delta\Phi^*$ and $\Delta\Phi = 1.5\Delta\Phi^*$, as in simulations we have observed that the jump in electrostatic potential across a shock can be up to $\approx$50% higher than given in Eq. (1) (see later). The two curves show that the reflection could be potentially significant and may be observable in simulations, providing a further motivation for our study.

The code used for our numerical experiments is the hybrid particle-in-cell code LSP.[16] Appendix A presents a series of benchmarks of the LSP collision operator, using both a thermalization problem and a slowing down problem. This gives us confidence that for our simulations LSP correctly describes Coulomb interactions among particles, to within the statistics allowed by our computational resources.

Our simulations show that collisions fundamentally change the character of the reflection problem. This is clearly demonstrated in Figs. 2(a) and 2(b), showing the phase-space for two simulations at M = 3.8 and M = 7.2: there is no clear signature of a reflected population of ions in the regions of the phase-space where they should be visible (denoted by the red arrows in Fig. 2). To estimate the statistical significance of this statement, consider that by the time of the two snapshots shown in Fig. 2, $\Delta t = 32$ ns and $\Delta t = 34$ ns, about 10^6 simulation particles (all with equal weights) had crossed the shock front, for both simulations. Next, we note that the time necessary to reach a steady state for the reflection mechanism can be considered to be the slowing down time of a reflected ion in the upstream plasma, Δt_s. For the M = 3.8 and M = 7.2 cases, we estimate

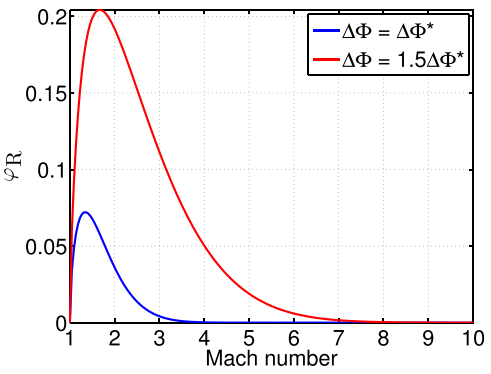

FIG. 1. Fraction of reflected ions φ_R as a function of Mach number and assuming $Z = 1$, if collisions are ignored.

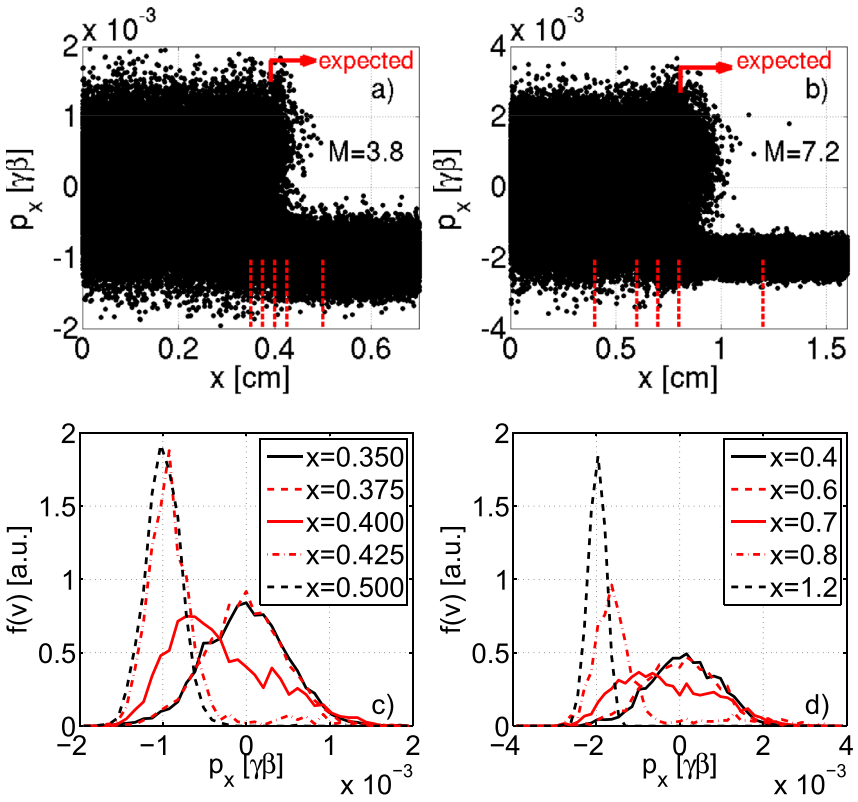

FIG. 2. Phase-space of average DT ions for a M = 3.8 (a) and M = 7.2 (b) shock propagating from left to right in a uniform plasma (flux limiter $f = 0.01$). Figures (c) and (d) show how the ion distribution function varies across the shock front (the chosen positions are also denoted with red broken lines in the phasespace plots). The arrows labeled "expected" denote regions in phase-space where one would expect to see ions reflected at the shock front. Snapshots taken at $t = 32$ ns (a,c) and $t = 34$ ns (b,d) from the beginning of the simulation.

$\Delta t_s = 0.7$ ns and $\Delta t_s = 1.7$ ns, respectively. Since we could at most identify only a few reflected particles $N_r \sim 10$ at any given time, we can conclude that ion reflection occurs in our simulations with a probability smaller than $N_r \Delta t / (\Delta t_s \times 10^6) \sim 10^{-4}$.

The shocks in the simulations were obtained by reflecting a flow of plasma particles against a wall at $x = 0$, a common technique used in the study of collisionless shocks,[14] so that the component of the momentum in the x direction changes sign as a particle collides against the wall. The plasma was composed of a single ion species with mass $m_i = 2.5\, m_p$ and charge state $+1$, where m_p is the proton mass. Hence, the ion particles represented an average $\langle DT \rangle$ ion species. The ions were treated as a kinetic species with binary collisions and the neutralizing electrons as a fluid species. The plasma was initialized with a velocity directed against the reflecting wall; the initial velocities, normalized with respect to the speed of light *in vacuo*, were set as $\beta = 1 \times 10^{-3}$ for the $M = 3.8$ case and $\beta = 2 \times 10^{-3}$ for the $M = 7.2$ case. The initial ion density was $n_i = 10^{20}\,\mathrm{cm}^{-3}$, there were 2500 ions/cell and the cell size was set smaller than the downstream ion-ion mean free path, for each distinct problem ($\Delta x = 20\,\mu$m for the case M = 3.8 and $\Delta x = 40\,\mu$m for the case M = 7.2).

That there is no clear signature of ion reflection at the shock front does not necessarily mean that there are no kinetic features in the ion distribution function. Panels c and d in Fig. 2 show the normalized distribution function of the ion species at different locations across the shock front. While the distribution function is symmetrical in the upstream and downstream regions, as expected, it transitions through a clearly non-Maxwellian distribution inside the shock. This could be due not only to the presence of an electric field but also to classical diffusion at the shock front as well as differential heating of the upstream ions.

Figure 3 shows the density and electric field profiles corresponding to the same simulations of Fig. 2. Two cases are displayed: one in which the flux limiter was set to $f = 0.01$ (broken lines) and one in which $f = 0.1$ (solid lines). As expected, when more electron heat flux is allowed to occur the shock profile presents a clearer density pedestal due to the electrons leaking ahead of the shock front and heating the upstream plasma. As this happens the electric field also changes its shape and shows a clear double-peak structure, which is already predicted from fluid theory.[15]

It would be interesting to compare these results against a fully kinetic calculation, in which also the electrons are treated as a kinetic species. In this case, the electron heat conduction would be automatically treated without the need for a flux limiter. However, this type of simulation would require significantly more computational power in order to conserve energy to a high degree (for the problems presented here, the energy was conserved to better than 99% level) and is left for future studies.

One of the features of ion-kinetic calculations is that the shock width is larger than predicted from fluid theory, an observation already made in Ref. 17 and later confirmed in Ref. 18. In order to compare our kinetic calculations with respect to fluid theory, we measured the ratio of the shock width observed in our simulations and compared it against the downstream ion-ion mean-free-path. In the simulations, we defined "shock width" as the distance over which the density increases from $\times 1.2$ of its upstream value to $\times 0.9$ of its downstream value. The choice of 1.2 was made in order to decrease the sensitivity to the value of the flux limiter, since as previously discussed, a higher value of the flux limiter

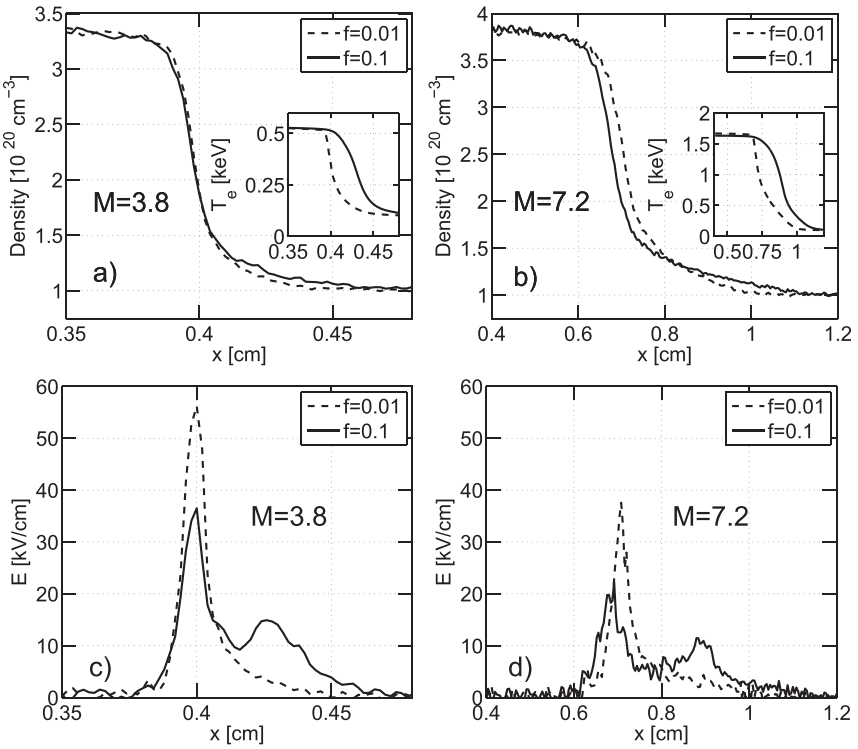

FIG. 3. Number density, electron temperature (insets), and electric field plots for M = 3.8 (a,c) and M = 7.2 (b,d) and for two different values of the flux limiter ($f = 0.01$ and $f = 0.1$). The shocks are propagating from left to right. Snapshots taken at $t = 32$ ns (a,c) and $t = 34$ ns (b,d) from the beginning of the simulation.

corresponds to a more pronounced pedestal in front of the ion viscous part of the shock (Figure 3). These values of the shock width were then compared against the fluid predictions obtained by integrating the equations in Ref. 15 (the equations within the "imbedded ion shock," in the words of Jaffrin and Probstein). The measured values were normalized against the ion-ion mean free path behind the shock, given by[19]

$$\lambda_{ii} = \frac{3}{4\sqrt{\pi}} \frac{T_i^2}{(Ze)^4 n_i \ln\Lambda}, \tag{4}$$

where all the relevant quantities are calculated in the downstream region of the shock and we used $\ln\Lambda = 23 - \ln\{Z^3(T_i[\mathrm{eV}])^{-3/2}(n_i[\mathrm{cm}^{-3}])^{1/2}\}$.[20]

Figure 4(a) presents the result of this analysis, for simulations in which the electron flux limiter was 0.01 and 0.1. As expected, the ion kinetic calculations (red and blue dots) are consistently higher than the fluid predictions (black line). Figure 4(b) shows the variation of the jump in electrostatic potential vs. Mach number. The estimate $\Delta\Phi^*$ is within a factor 1.5 of the simulation results. The simulations used for the plots in Fig. 4 include the cases M = 3.8 and M = 7.2 previously discussed. The other simulations were obtained by changing the velocity of the beam directed against the reflecting wall, while keeping all the other parameters the same.

The fact that there is no clear ion reflection at the shock front is not limited to the cases displayed in Figs. 2 and 3. Indeed, no clear signatures of ion reflection are observed for other simulations with Mach numbers M = 2.2, M = 5.4, and M = 10.8 with the same background density.

To make the argument about ion reflection more compelling and generalize the simulation results to different Mach numbers and background density, we make the following consideration. The figure of merit that must be considered is the ratio of the mean free path of the reflected ions, over the width of the shock front. At this point, our reasoning can be cast in the form of a null hypothesis test: if the ion dynamics were dominated by the electric field at the shock front, ions with kinetic energy below the threshold $(2Ze\Delta\Phi/m_i)^{1/2}$ would slow down on the way to their respective turning point distance, and then be accelerated back

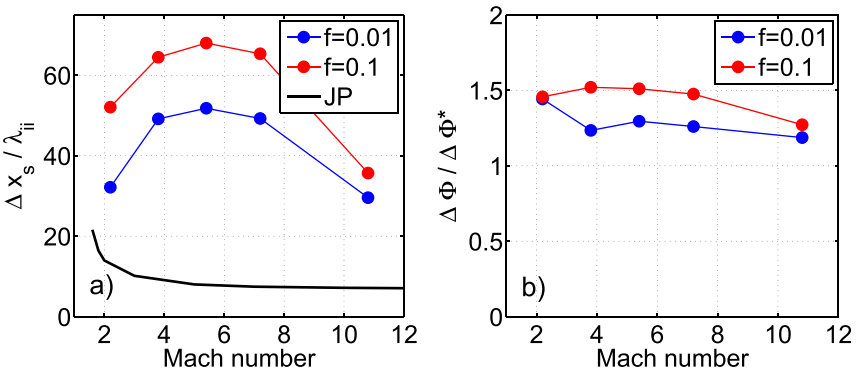

FIG. 4. Dependence of the normalized shock width (a) and electrostatic potential (b) with Mach number. Upstream number density: $n_{\langle DT\rangle} = n_e = 10^{21}\,\mathrm{cm}^{-3}$; upstream temperature: $T_{\langle DT\rangle} = T_e = 100\,\mathrm{eV}$. The black line is obtained from the fluid theory developed in Ref. 15. The lines connecting the simulation points in blue and red serve as a guide for the eye.

towards the upstream region. However, we will show that in this circumstance, ions would undergo so many collisions to invalidate the original hypothesis that the electric field dominates the ion dynamics.

It is important to stress that by no means are the ion trajectories expected to follow the above description, the one depicted as a sketch in Fig. 5. In this sense our treatment should just be seen as illustrative, serving the point of understanding the importance of collisions for this problem.

In order to estimate how many collisions the potentially reflected ions will undergo while reflected at the shock front, we use the slowing down formula for "slow" ions, $v_i < (k_B T_i/m_i)^{1/2} \ll (k_B T_e/m_e)^{1/2}$, for which the slowing down frequency ν_s is approximately independent of the initial ion velocity[20,21]

$$\nu_s \approx \frac{16\sqrt{2\pi}(Ze)^4 n_i \ln\Lambda}{3 m_i^{1/2} T_i^{3/2}}. \tag{5}$$

This choice is justified by the fact that reflection is most likely to occur at low Mach numbers (Fig. 1). Particularly in this low Mach number regime, the difference in velocity Δv between the most energetic upstream reflected ions and the downstream bulk plasma is $\Delta v = \sqrt{2Ze\Delta\Phi/m_i} - v_2 \lesssim 1$.

To calculate the (field-free) ion mean-free-path, $\lambda_{m.f.p.}$, we use the equation $dv_i/dt = -\nu_s v_i$, from which $\lambda_{m.f.p.} = \lim_{t\to\infty} x_i(t) = v/\nu_s$, where v is the initial ion velocity. Denoting with $\Delta x_{t.p.}$ the turning point distance, the probability that potentially reflected ions do not collide at the shock front (where there is an electric field) before reaching the turning point can then be estimated as

$$\mathrm{P(no\text{-}collision)} = \max\left(0, 1 - \frac{\Delta x_{t.p.}}{\lambda_{m.f.p.}}\right). \tag{6}$$

The quantity $\Delta x_{t.p.}$ can be calculated by equating the electrostatic potential energy with the ion kinetic energy, $Ze\Delta\Phi_{t.p.} = 1/2 m_i v^2$ and then, assuming for simplicity that the potential increases linearly within the shock front

$$\Delta x_{t.p.} \approx \frac{\Delta\Phi_{t.p.}}{\Delta\Phi}\Delta x_s = \frac{m_i v^2}{2Z\Delta\Phi}\Delta x_s \approx \frac{(v/v_{th,1})^2}{2Z\, T_2/T_1 \ln(\rho_2/\rho_1)}\Delta x_s, \tag{7}$$

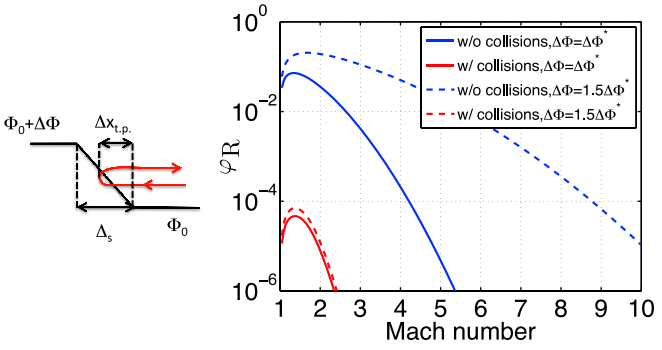

FIG. 5. (Left) Sketch showing the mechanism of ion reflection, if collisions were negligible. (Right) Estimated fraction of reflected ions φ_R as a function of Mach number, without (blue curves) and with (red curves) collisions and for two different values of the electrostatic potential ($\Delta\Phi = \Delta\Phi^*$ and $\Delta\Phi = 1.5\Delta\Phi^*$).

where the last equality was obtained using Eq. (1) (i.e., assuming $\Delta\Phi \approx \Delta\Phi^*$). In Eq. (7), Δx_s is the shock width, $v_{th,1}$ is the upstream ion thermal velocity and T_2/T_1, ρ_2/ρ_1 are the ratios of post- and pre-shock temperatures and densities; from the Rankine-Hugoniot relations, they are only a function of the Mach number of the shock.

The quantity Δx_s is a multiple μ of the ion-ion mean free path in the shocked region, $\Delta x_s = \mu\lambda_{ii}$, where $\mu > 1$ (Fig. 4(a)). Using $\lambda_{m.f.p.} = v/\nu_s$, post-shock expressions for Eqs. (4) and (5), and also using Eq. (7), Eq. (6) can be rewritten as

$$\mathrm{P(no\text{-}collision)} = \max\left(0, 1 - \frac{2\sqrt{2}\mu}{Z(T_2/T_1)^{1/2}\ln(\rho_2/\rho_1)}\frac{v}{v_{th,1}}\right). \tag{8}$$

The equation above predicts that ions with higher velocity are more likely to collide at the shock front, the reason being that they have to travel a longer distance before being reflected by the electric field. Moreover, our choice for the expression of the slowing down frequency is independent of the initial velocity; other expressions will yield a different formal dependence on $v/v_{th,1}$.

At this point Eq. (8) can be used as a "weight" function, transforming Eq. (3) as

$$\varphi_R = \frac{\int_0^{\sqrt{2Ze\Delta\Phi/m_i}} f(v)\mathrm{P(no\text{-}collision)}(v)\mathrm{d}v}{\int_{-\infty}^{+\infty} f(v)\mathrm{d}v}.$$

The result of this integration, as a function of Mach number, is presented in Fig. 5. The blue curves are the same as the ones in Fig. 1, except that the y-axis is now in log scale. When collisions are included (red curves), the reflected fraction decreases by several orders of magnitude.

In conclusion, these estimates show that collisions significantly alter the ion dynamics at the shock front, for any Mach number and, to first order, independently of the background density. Hence the presence of collisions invalidate the "collisionless" notion that, in the lab frame, ions reflected at the shock front gain speeds equal to twice the shock speed.

Different results may be obtained in problems which involve inhomogeneous plasmas. For example, when the shock is produced from an initial discontinuity, the ion phase space resembles the one for a collisionless shock,[22] due to the presence of an electric field at the interface that drives the acceleration of ions in a kinetic fashion. When a shock traverses an interface that separates a plasma with two different thermodynamic conditions, we also observe strong features of a non-Maxwellian ion distribution function that can lead to significant mixing of ions close to the interface.

III. KINETIC SIMULATIONS OF SPECIES SEPARATION IN SPHERICAL GEOMETRY

Multi-fluid calculations of ICF implosions in spherical geometry have been shown in Ref. 8, demonstrating the separation of D and T ions as the shock converges towards the

center of an ICF capsule. Ion-kinetic calculations of D^3He gas target implosions, using a Vlasov-Fokker-Planck approach, have also been presented.[23]

Here we present results in a similar context as in Ref. 8, using a collisional particle-in-cell description of the ion dynamics and assuming, as before, fluid electrons. The objective is to compare results between an average-ion-species and a multi-ion-species description. Our kinetic results confirm the possibility of separation of D and T ions in the gas, during ICF implosions, in agreement with our earlier results using a multi-fluid approach.

In order to compare the average-ion-species and two-ion-species calculations, the initial mass density and number density were kept the same, $\rho_{\langle 12\rangle} = \rho_1 + \rho_2$ and $n_{\langle 12\rangle} = n_1 + n_2$, where the subscript $\langle 12\rangle$ refers to the average species. The mass of the average species must then be chosen as

$$m_{\langle 12\rangle} = \alpha_1 m_1 + \alpha_2 m_2 \,, \tag{9}$$

where $\alpha_{1,2}$ represent the concentrations of the two species, $\alpha_i = n_i / \sum_j n_j$.

The simulation to be discussed in this section was obtained after starting from a 1D spherical HYADES[24] simulation of a laser-driven ICF implosion, for conditions achievable at the OMEGA laser facility. The shell was made of C and D atoms with a thickness of 5.1 μm and a diameter of 880 μm; the atomic fraction of C and D atoms was 41.7:58.3. The gas fill was assumed to be a 50:50 mixture of D and T atoms. The initial electron density in the gas region was $n_e = 2.35 \times 10^{19}\,\mathrm{cm}^{-3}$, corresponding to a mass density $\rho_{gas} = 0.1\,\mathrm{mg/cm}^3$.

The 1D spherical LSP simulation was started by taking the HYADES data at $t_0 = 0.9$ ns. At this time, the shock produced at the plasma ablation front had already entered the gas region. After this time, the laser driver is over and the rest of the solution is then evolved with the kinetic calculation. The LSP simulations were initialized with kinetic average-CD ions $\langle CD\rangle$ and either separate kinetic D and T ions or average-DT ions $\langle DT\rangle$, with 5000 particles/cell for each species. As before, the electrons were assumed to be a fluid species. The charge state for the $\langle CD\rangle$ species was +3, while the D, T and $\langle DT\rangle$ species had a charge state of +1. An ideal equation of state was used to close the system of equations and a flux limit $f = 0.06$ was used throughout the simulation domain. Using Eq. (9), the average masses were chosen as $m_{\langle DT\rangle} = (m_D + m_T)/2$ and $m_{\langle CD\rangle} = 0.42\,m_C + 0.58\,m_D$.

Figure 6 presents the results at two snapshots of the particle-in-cell (PIC) calculation. In the left column, the shock is about to reach the center at $r = 0$, while in the right column, the shocks have all reached the center for both calculations (D, T ions and $\langle DT\rangle$ ions) and the density has increased by one to two orders of magnitude. Overall, the number density of the average-species calculation (black curves in Figs. 6(a) and 6(b) appears to be close to the sum of the densities of the D and T ions (green curves in Figs. 6(a) and 6(b)), $n_{\langle DT\rangle} \approx n_D + n_T$. However, the time of arrival of the $\langle DT\rangle$ species at $r = 0$ is later than the D species (by about 50 ps) and earlier than the T species (by 50 to 100 ps). It is also interesting to note how the $\langle DT\rangle$ ion temperature lies in between the D and T temperatures.

As noted before,[8] since in a two-species calculation the D and T ions are out of phase around shock flash in terms of timing of both peak densities and temperatures, there should be a signature of species separation in the fusion burn history. Further work is necessary in order to extend our current ion-kinetic simulations well past shock flash and understand these effects in more detail.

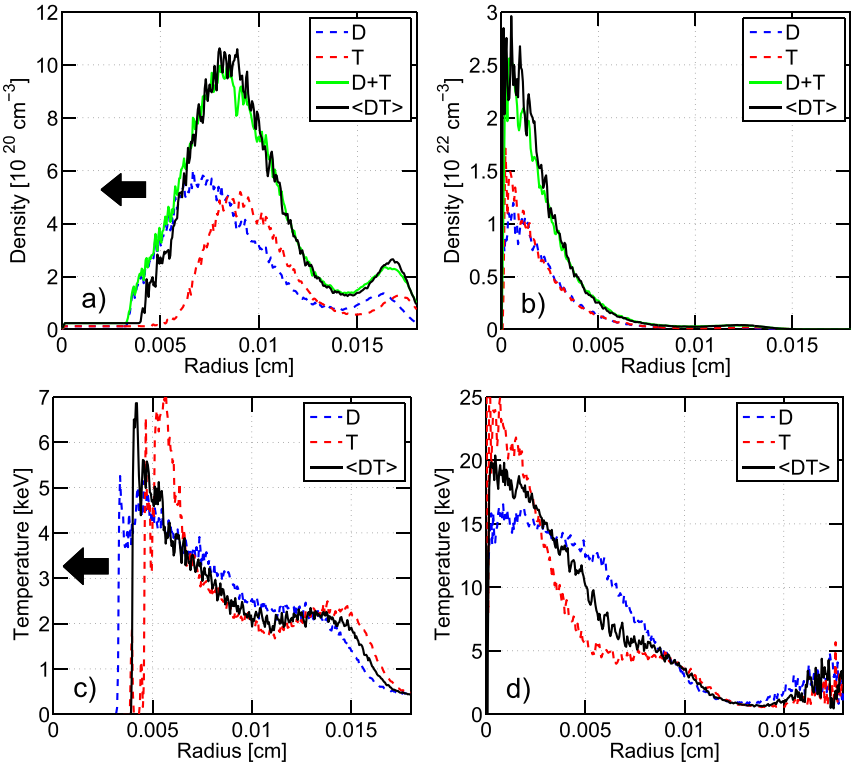

FIG. 6. Plots of number density and temperature at $t = t_0 + 0.18$ ns (a,c) and $t = t_0 + 0.23$ ns (b,d), where t_0 denotes the beginning of the LSP simulation. The kinetic, average-CD ion species is not shown.

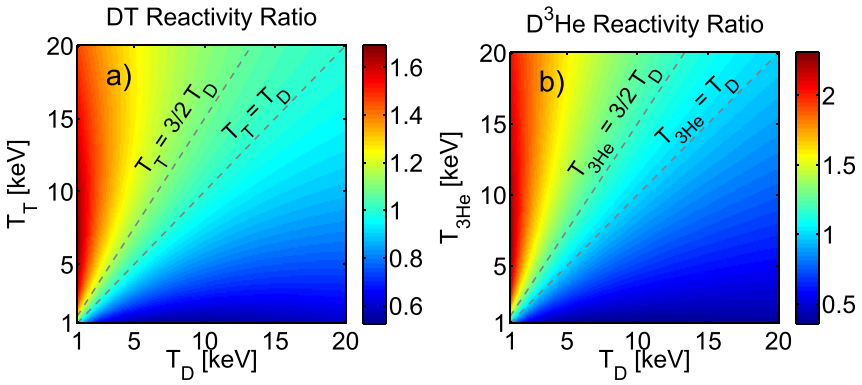

FIG. 7. Ratio of fusion reactivities $R_{\langle\sigma v\rangle}$, for the cases of (a) DT mixture and (b) D^3He mixture. The reactivities are calculated using the coefficients in Bosch and Hale.[26,27]

IV. EFFECT OF DIFFERENTIAL ION TEMPERATURE ON FUSION YIELD

Multi-fluid calculations are the natural extension of current single-fluid calculations for ICF implosions. With a multi-fluid code, the ion species are allowed to have different temperatures and Figs. 6(c) and 6(d) demonstrate that this circumstance is quite plausible during ICF implosions. Leaving aside the question of whether or not approximating the distribution function with a Maxwellian is reasonable, an interesting question is how having different D and T temperatures impacts the fusion yield and hence the experimental observables. As it turns out, it is possible to give a simple expression for the fusion reactivity, for the case of two Maxwellian ion distributions with different temperatures. During the review of this manuscript we were made aware that this calculation was already done by Brysk in 1973.[25] Since our approach to the problem is different and possibly more transparent, we have added our derivation to Appendix B for the benefit of the reader.

The important result is that if ions 1 and 2 have temperatures T_1 and T_2, the fusion reactivity can be simply evaluated using an effective temperature $T_{\rm eff}$

$$T_{\rm eff} = \frac{m_1 T_2 + m_2 T_1}{m_1 + m_2}\,. \tag{10}$$

For DT and D^3He mixtures, the effective temperature $T_{\rm eff}$ and the average temperature $T_{\rm av} = (T_1 + T_2)/2$ differ by less than 20% in the range 1–20 keV. However, the ratio of the fusion reactivity calculated using the effective temperature and the average temperature, $R_{\langle\sigma v\rangle} = \langle\sigma v\rangle(T_{\rm eff})/\langle\sigma v\rangle(T_{\rm av})$, can be substantially different from 1 for unequal temperatures (Fig. 7); hence Eq. (10) should be used in this case.

The quantity $T_{\rm av}$ can be regarded as a first-order estimate of the average-species temperature solution for the case of an equi-molar mixture of D and T ions. Indeed, as a rough assumption we can assume that the shock speeds for the D and T ions, in a 2-species calculation, and $\langle$DT$\rangle$ ions, in an average-species calculation, are all the same, $v_{\rm sh}$. Immediately behind the shocks, and before the temperatures have equilibrated to the downstream solution, the kinetic energy of each species α is transformed into thermal energy, so that $k_B T_\alpha \sim m_\alpha v_{\rm sh}^2/2$. This means that for D and T, the temperature ratio just behind the shock is $T_T/T_D \sim 3/2$. Further downstream the shock front, the species (including the electrons) will then equilibrate to the downstream temperature T_2. Using this same argument, an average-species calculation would instead yield a solution $k_B T_{\langle\rm DT\rangle} \sim m_{\langle\rm DT\rangle} v_{\rm sh}^2/2 = [(m_D + m_T)/2] v_{\rm sh}^2/2 \sim k_B T_{\rm av}$ immediately behind the shock, before converging also to T_2.

It is instructive to evaluate the fusion reactivity using $T_{\rm eff}$ and $T_{\rm av}$ when $T_T/T_D = 3/2$ and also $T_{3He}/T_D = 3/2$. Along this line, plotted in Fig. 7, $R_{\langle\sigma v\rangle} = 1.06 - 1.20$ for DT and $R_{\langle\sigma v\rangle} = 1.15 - 1.30$ for D^3He, this ratio being larger at lower temperatures. For reference, in the same figures two lines at $T_T/T_D = 1$ and $T_{3He}/T_D = 1$ are also plotted, for which $R_{\langle\sigma v\rangle} = 1.0$.

As a practical application, we use the same multi-fluid calculation shown in Fig. 9(d) of Ref. 8 and evaluate the DT fusion rate using the coefficients given by Bosch and Hale.[26,27] Note that the fusion burn rate depends on the density as well, not just the temperature. Figure 8 shows how the DT fusion rate varies for different choices of the DT temperature. For this specific simulation, using the average temperature gives a fusion rate that is within 5% of the one calculated using $T_{\rm eff.}$ If the reference temperatures were the deuteron and triton temperature, T_D and T_T, the resulting curves would differ from the blue curve by up to 20%. Note that in this figure the green broken curve, associated with T_D, is higher than the black broken one, associated with T_T, during the first peak (shock yield). The reverse happens during the second peak of the fusion reactivity curve (compression

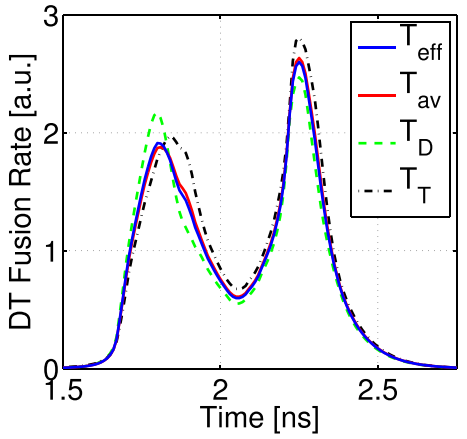

FIG. 8. DT fusion rate vs. time, for the simulation presented in Fig. 9(d) of Ref. 8. The different curves show the sensitivity of the burn history on the choice of the reference temperature.

yield), which is instead associated with the deceleration of the shell. This is due to the fact that the deuterons arrive first at the center, so that the D ions are initially hotter than the T ions; later in time, the T ions are instead the hottest.

It is important to stress that the purpose of Fig. 8 is to show the sensitivity of the fusion burn rate on the choice of the reference temperature (the correct one being $T_{\rm eff}$). The result of a single-fluid calculation cannot be extrapolated from these curves. Indeed, Fig. 9(c) of Ref. 8 shows that a single-fluid calculation yields a significantly different burn history.

V. CONCLUSIONS

In this paper we have presented ion-kinetic calculations of shocks for conditions relevant to ICF studies.

It was shown that a steady shock propagating in a uniform plasma in slab geometry does not present signatures of ion reflection at the shock front, due to collisions. The distribution function across the shock front shows, however, departures from a Maxwellian distribution function. While the shock width was shown to be significantly larger than from fluid theory, the jump in electrostatic potential is well described, within a factor of 1.5, by the estimate given in Eq. (1).

In spherical geometry and for conditions close to ICF experiments on OMEGA, ion-kinetic calculations confirm the possibility of species separation of D and T ions. An average-species calculation seems to compare favorably against a two-species calculation, but the different timing of peak density and temperature in a multi-species calculation makes the case for continuing investigating these effects for ignition-relevant experiments.

Since species separation implies also different temperatures for different ion species, some of the implications of this for fusion burn calculations were addressed. In general, an effective temperature $T_{\rm eff}$ should be used in multi-fluid codes, as opposed to a simple average of the temperatures. Depending on the parameters, this may or may not make a difference in the interpretation of experimental results.

ACKNOWLEDGMENTS

C.B. acknowledges useful discussions with B. Cohen and A. Dimits on the collision operator in particle-in-cell codes and with D. Ryutov on the fusion reactivity. Computing support for this work came from the Lawrence Livermore National Laboratory (LLNL) Institutional Computing Grand Challenge program. This work was performed under the auspices of the U.S. Department of Energy by the Lawrence Livermore National Laboratory under Contract No. DE-AC52-07NA27344 and supported by LDRD-11-ERD-075.

APPENDIX A: BENCHMARKS

In this section, we present several benchmarks of the collision operator implemented in the parallel, hybrid, electromagnetic simulation code LSP.[16] The core plasma physics of the code is described by a particle-in-cell description of the species, treated as either kinetic or fluid, which interact with each other via Coulomb collisions. The collision operator for the kinetic species is the binary Takizuka-Abe operator,[28] implemented using Nanbu's algorithm.[29] The tests were made using both a standard thermalization problem and a slowing down problem.

In all tests presented in this section, the simulations were initialized with one cell and N particles/species within the cell. No particle motion was allowed. Moreover, the same value $\ln\Lambda = 10$ was forced for all interactions, in order to better compare the results with analytic theory.

Regarding the first test, given a Maxwellian population of ion and electron species at rest and with different initial temperatures, the species will relax to the same temperature in a time dictated by collisions among particles. In a fluid approximation, the temperature of species α should vary with time as

$$\frac{{\rm d}T_\alpha}{{\rm d}t} = \sum_{\beta\neq\alpha} \nu^{\alpha\beta}(T_\beta - T_\alpha)\,, \tag{A1}$$

where the summation is over all the other species β and the relaxation frequency $\nu^{\alpha\beta}$ is given by[20]

$$\nu^{\alpha\beta} = 1.8\times10^{-19}\,\frac{(m_\alpha m_\beta)^{1/2} Z_\alpha^2 Z_\beta^2 n_\beta \ln(\Lambda_{\alpha\beta})}{(m_\alpha T_\beta + m_\beta T_\alpha)^{3/2}}\ {\rm s}^{-1}\,.$$

At first, we performed the same test proposed by Rambo and Procassini.[30] For this test, the mixture is composed of two kinetic carbon species with charge state +6, each with number density $n_{\rm C} = 1\times10^{20}{\rm cm}^{-3}$. One of the species is initialized with a temperature of 1 keV, the other with a temperature of 250 eV. As time progresses, the two species relax to the same temperature, Fig. 9(a). The time resolution for this problem was $\Delta t = 1$ fs and Fig. 9(a) presents two cases in which the number of particles/species were $N = 5000$ and $N = 20\,000$, with little difference between the two curves. The results are in fact in good agreement with those of Ref. 30. The apparent disagreement between the fluid and kinetic solution is explained by the fact that the fluid solution simply cannot capture the slow equilibration of high-energy particles, as observed in the same reference.[30] Good agreement is only expected at early times, as it will be the case for the slowing down problem.

As a second test, we initialized a thermalization problem with two ion kinetic species and fluid electrons. The objective was to be closer to the typical parameters of our simulations. For this test, the ion species were kinetic D and T ions with initial temperatures of 3 keV and 5 keV, respectively, and either $N = 5000$ or $N = 20\,000$. The fluid electrons were initialized with a temperature of 1 keV and density $n_{\rm e} = 2\times10^{20}\,{\rm cm}^{-3}$. For each simulation, the ion density was chosen so as to neutralize the electric charge, and assuming the same number density for both ion species (so that $n_{\rm D} = n_{\rm T} = 1\times10^{20}\,{\rm cm}^{-3}$). The time resolution was $\Delta t = 50$ ps. Figure 9(b) shows the result of this test. As before, the kinetic curves are in good agreement with the fluid results at early times and (obviously) also at late times. They are not supposed to be in perfect agreement in between these two limits.

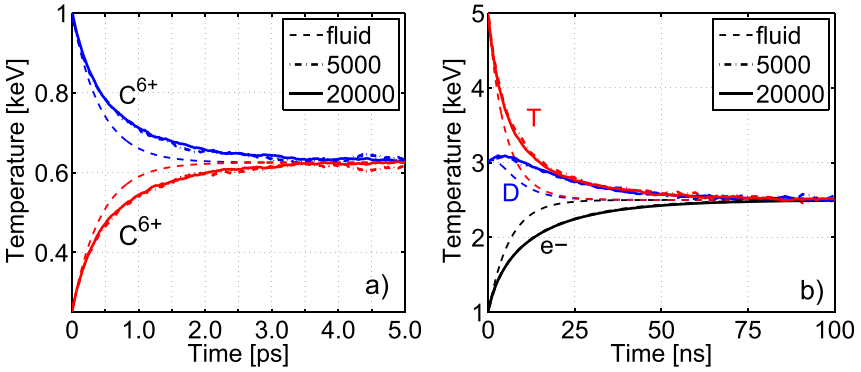

FIG. 9. Thermalization tests with (a) C^{6+}, C^{6+} kinetic ions and (b) D, T, e^- kinetic ions and fluid electrons. Two particle-in-cell solutions are plotted in each panel, for two different choices of the number of particles/species ($N = 5000$ and $N = 20\,000$). Little difference is observed for these two choices.

For the slowing down problem, we compare our simulations with a reduced model of the Vlasov-Fokker-Planck equation. We study how a test ion with velocity u_α, charge q_α, and mass m_α is slowed down in a Maxwellian plasma composed of ions/electrons with mass m_β and temperature T_β. We solve directly the equation given by Trubnikov[31]

$$\frac{\mathrm{d}\langle u_\alpha\rangle}{\mathrm{d}t} = -\nu_s^{\alpha\beta}\langle u_\alpha\rangle, \tag{A2}$$

where the operator $\langle\cdot\rangle$ denotes an average over the distribution function and, after defining $\xi^* = m_\beta v_\alpha^2/(2k_B T_\beta)$, the slowing down collision frequency is given by

$$\nu_s^{\alpha\beta} = \frac{8\sqrt{\pi}q_\alpha^2 q_\beta^2 n_\beta \ln\Lambda_{\alpha\beta}}{m_\alpha^2 v_\alpha^3}\left(1+\frac{m_\alpha}{m_\beta}\right)\int_0^{\xi^*}\mathrm{d}\xi\,\xi^{1/2}\exp(-\xi)\,.$$

Equation (A2) is a classic reference in plasma physics and it is also given by the NRL formulary.[20]

It is important to understand that this equation neglects diffusion of the test beam in velocity space, as the test beam is always assumed to be described by a Dirac function in velocity space. While this is a good assumption at early times, at later times the spreading of the test beam in velocity space starts to affect the solution. Hence, the particle-in-cell results are only expected to agree with Eq. (A2) at early times. For comparison at later times, the full Vlasov-Fokker-Planck equation should be solved.

Two test cases are examined, which are both relevant to our simulations. For both cases, the density of the test particle beam was set to a negligible value in comparison to the background density, $n_T = 10^8\,\mathrm{cm}^{-3}$, so that the choice of this parameter did not affect the solution. In the first test, we benchmarked how kinetic ions are slowed down by other kinetic ions. A population of kinetic T ions (tritons) was initialized with a velocity $\beta = 10^{-4}$, normalized against the speed of light in vacuum, and no initial spread in energy. The background particles were made of kinetic D ions (deuterons) with initial temperature $T_D = 100\,\mathrm{eV}$ and density $n_D = 10^{21}\,\mathrm{cm}^{-3}$. Figure 10(a) presents the results of this test case. The early time solution is in excellent agreement with Eq. (A2), while it departs from it at later times, when diffusion cannot be neglected. Three curves are presented with $N = 20\,000$, 40 000, and 160 000.

Although the number of particles per cell used for these tests is larger than the one used in the shock simulations presented in Sec. II, the particle statistics of Sec. II is good: no significant differences were observed when the simulations were run with 10 000 (as opposed to 2500) particles/cell. There may be several reasons for this, including the fact that by the time the solutions reached a nearly steady state, the shocks had travelled for many cells (on the order of a hundred), thus lowering statistical fluctuations behind the shock front significantly.

For the second test, we examine the slowing down of kinetic ions due to fluid electrons. The normalized velocity of the beam of T ions was $\beta = 10^{-2}$ (with no spread in energy). The fluid electrons were initialized with $T_e = 10\,\mathrm{eV}$ and $n_e = 10^{21}\,\mathrm{cm}^{-3}$. The results are shown in Fig. 10(b). There was little dependence of the results on the choice of the particle number, hence in the figure only the case $N = 1000$ is shown.

These test cases exhaust all the possible scenarios for the slowing down of ions in a collisional shock. Indeed, in this case the ions are expected to be slowed down mostly by electrons in the thermal pedestal ahead of the shock, provided that enough electron thermal conduction is allowed by the value of the flux limiter. At the shock front, instead, ion-ion collisions are the dominant mechanism for losing directed kinetic energy into thermal energy.[18]

APPENDIX B: GENERALIZATION OF FUSION REACTIVITY TO DIFFERENT ION TEMPERATURES

In this Appendix we present a simple formula that generalizes the fusion reactivity to the case of two Maxwellian ion populations with different temperatures. This is an independent, and alternative, derivation from the one given by Brysk.[25] A related problem, which was focused on understanding the distribution of the fusion products, was covered in Ref. 32.

In order to study this problem, we start by assuming that species i has a Maxwellian velocity distribution function given by

$$f_i(\mathbf{v}) = \left(\frac{m_i}{2\pi k_B T_i}\right)^{3/2}\exp\left(-\frac{m_i|\mathbf{v}|^2}{2k_B T_i}\right).$$

The standard fusion reactivity formula can be written as

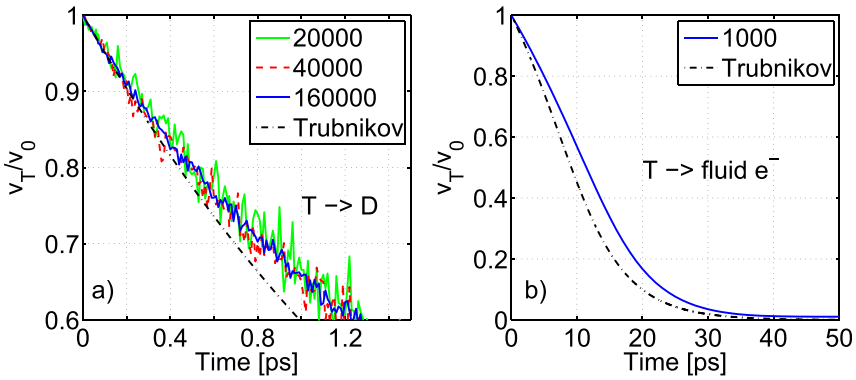

FIG. 10. Slowing down test cases. (a) Slowing down of T ions in a background of D ions. (b) Slowing of down of T ions in a background of fluid electrons. The variable v_T/v_0 is the velocity of the test particle, normalized to its initial value. For the numerical parameters of these test cases, see the supporting text.

$$\langle \sigma v \rangle = \int \mathrm{d}^3\mathbf{v}_1 \mathrm{d}^3\mathbf{v}_2 \, \sigma(|\mathbf{v}_1 - \mathbf{v}_2|)|\mathbf{v}_1 - \mathbf{v}_2| f_1(\mathbf{v}_1) f_2(\mathbf{v}_2). \quad \text{(B1)}$$

Since the cross section σ depends on the relative velocity between the two ion species, we want to find a transformation of variables that leads to the integration over $\mathbf{v}_1 - \mathbf{v}_2$. Usually, the ion velocities are written as the sum of the center of mass velocity and a term proportional to the relative velocity.[27] Here we will show that a more convenient linear combination exists, for the case of our interest.

We start by writing the following, general change of variables from $\mathbf{v}_1$ and $\mathbf{v}_2$ to $\mathbf{v}_a$ and $\mathbf{v}_b$:

$$\mathbf{v}_1 = a_1 \mathbf{v}_a + b_1 \mathbf{v}_b, \quad \text{(B2)}$$

$$\mathbf{v}_2 = a_2 \mathbf{v}_a + b_2 \mathbf{v}_b. \quad \text{(B3)}$$

Using this transformation, the exponential resulting from the product $f_1(\mathbf{v}_1) f_2(\mathbf{v}_2)$ is given by

$$\exp\left(-\frac{1}{2}\frac{m_1 v_1^2}{k_\mathrm{B} T_1} - \frac{1}{2}\frac{m_2 v_2^2}{k_\mathrm{B} T_2}\right) = \exp\left[-v_a^2\left(\frac{m_1 a_1^2}{2k_\mathrm{B} T_1} + \frac{m_2 a_2^2}{2k_\mathrm{B} T_2}\right)\right., \quad \text{(B4)}$$

$$\left. - v_b^2\left(\frac{m_1 b_1^2}{2k_\mathrm{B} T_1} + \frac{m_2 b_2^2}{2k_\mathrm{B} T_2}\right) - v_a v_b\left(\frac{m_1 a_1 b_1}{k_\mathrm{B} T_1} + \frac{m_2 a_2 b_2}{k_\mathrm{B} T_2}\right)\right]. \quad \text{(B5)}$$

At this point, the coefficients $a_{1,2}$ and $b_{1,2}$ can be chosen so that the last term in the previous equation is equal to zero. Since this is the only constraint in the transformation of variables given above, there are still three degrees of freedom in choosing the values of the coefficients. Our choice is to impose $a_1 = a_2 = b_1 = 1$ and the value of b_2 must instead satisfy the condition $b_2 = -(m_1 T_2)/(m_2 T_1)$. After solving the system of Eqs. (B2) and (B3) with the coefficients given above, it is then straightforward to find that the variables $\mathbf{v}_a$ and $\mathbf{v}_b$ are given by

$$\mathbf{v}_a = \frac{m_1 T_2 \mathbf{v}_1 + m_2 T_1 \mathbf{v}_2}{m_1 T_2 + m_2 T_1}, \quad \text{(B6)}$$

$$\mathbf{v}_b = \frac{m_2 T_1}{m_1 T_2 + m_2 T_1}(\mathbf{v}_1 - \mathbf{v}_2). \quad \text{(B7)}$$

The value $\mathbf{v}_a$ above is a weighted center-of-mass velocity. The standard expression can be recovered in the limit of equal temperatures. Similarly, the quantity $\mathbf{v}_b$ is proportional to the relative velocity of the two ion species, as desired. In the same limit of equal temperatures, one recovers the usual coefficient in front of $(\mathbf{v}_1 - \mathbf{v}_2)$.

The fusion reactivity can now be written as

$$\langle \sigma v \rangle = \left(\frac{m_1}{2\pi k_\mathrm{B} T_1}\right)^{3/2}\left(\frac{m_2}{2\pi k_\mathrm{B} T_2}\right)^{3/2}\int \mathrm{d}^3\mathbf{v}_1 \mathrm{d}^3\mathbf{v}_2 \sigma(|\mathbf{v}_1 - \mathbf{v}_2|) \quad \text{(B8)}$$

$$|\mathbf{v}_1 - \mathbf{v}_2| \exp\left[-\frac{v_a^2}{2}\left(\frac{m_1}{k_\mathrm{B} T_1} + \frac{m_2}{k_\mathrm{B} T_2}\right) - \frac{m_\mathrm{r}|\mathbf{v}_1 - \mathbf{v}_2|^2}{2k_\mathrm{B} T_\mathrm{eff}}\right], \quad \text{(B9)}$$

where we have introduced the reduced mass $m_\mathrm{r} = m_1 m_2/(m_1 + m_2)$ and we have defined an effective temperature

$$T_\mathrm{eff} = \frac{m_1 T_2 + m_2 T_1}{m_1 + m_2}. \quad \text{(B10)}$$

At this point, the derivation follows the standard procedure. The Jacobian determinant of the transformation $\mathbf{v}_1 \to \mathbf{v}_a$, $(\mathbf{v}_1 - \mathbf{v}_2)$ and $\mathbf{v}_2 \to \mathbf{v}_a$, $(\mathbf{v}_1 - \mathbf{v}_2)$ is equal to 1, so that the integral in $\mathrm{d}^3\mathbf{v}_1 \mathrm{d}^3\mathbf{v}_2$ can be simply replaced by an integral in $\mathrm{d}^3\mathbf{v}_a \mathrm{d}^3(\mathbf{v}_1 - \mathbf{v}_2)$. After following the same procedure as in Ref. 27, the final expression for the fusion reactivity is then

$$\langle \sigma v \rangle = 4\pi\left(\frac{m_\mathrm{r}}{2\pi k_\mathrm{B} T_\mathrm{eff}}\right)^{3/2}\int_0^\infty \mathrm{d}v \sigma(v) v^3 \exp\left(-\frac{m_\mathrm{r} v^2}{2k_\mathrm{B} T_\mathrm{eff}}\right), \quad \text{(B11)}$$

where $v = |\mathbf{v}_1 - \mathbf{v}_2|$. This shows that the reactivity for two Maxwellian ion distribution functions with different temperatures can be readily obtained in the usual fashion, except that the temperature to be used is the effective temperature given by Eq. (B10). Equation (B11) is identical to Eq. (B15) in Ref. 25.

[1]J. R. Rygg, F. H. Séguin, C. K. Li, J. A. Frenje, M. J.-E. Manuel, R. D. Petrasso, R. Betti, J. A. Delettrez, O. V. Gotchev, J. P. Knauer, D. D. Meyerhofer, F. J. Marshall, C. Stoeckl, and W. Theobald, "Proton radiography of inertial fusion implosions," Science **319**(5867), 1223–1225 (2008).
[2]C. K. Li, F. H. Séguin, J. R. Rygg, J. A. Frenje, M. Manuel, R. D. Petrasso, R. Betti, J. Delettrez, J. P. Knauer, F. Marshall, D. D. Meyerhofer, D. Shvarts, V. A. Smalyuk, C. Stoeckl, O. L. Landen, R. P. J. Town, C. A. Back, and J. D. Kilkenny, "Monoenergetic-proton-radiography

measurements of implosion dynamics in direct-drive inertial-confinement fusion," Phys. Rev. Lett. **100**, 225001 (2008).
[3]J. R. Rygg, J. A. Frenje, C. K. Li, F. H. Séguin, R. D. Petrasso, J. A. Delettrez, V. Yu Glebov, V. N. Goncharov, D. D. Meyerhofer, S. P. Regan, T. C. Sangster, and C. Stoeckl, "Tests of the hydrodynamic equivalence of direct-drive implosions with different D2 and He3 mixtures," Phys. Plasmas **13**(5), 052702 (2006).
[4]D. T. Casey, J. A. Frenje, M. Gatu Johnson, M. J.-E. Manuel, H. G. Rinderknecht, N. Sinenian, F. H. Séguin, C. K. Li, R. D. Petrasso, P. B. Radha, J. A. Delettrez, V. Yu Glebov, D. D. Meyerhofer, T. C. Sangster, D. P. McNabb, P. A. Amendt, R. N. Boyd, J. R. Rygg, H. W. Herrmann, Y. H. Kim, and A. D. Bacher, "Evidence for stratification of deuterium-tritium fuel in inertial confinement fusion implosions," Phys. Rev. Lett. **108**, 075002 (2012).
[5]M. Rosenberg *et al*., Phys. Rev. Lett. **112**, 185001 (2014).
[6]H. Rinderknecht *et al*., Phys Rev. Lett. **112**, 135001 (2014).
[7]P. Amendt, S. C. Wilks, C. Bellei, C. K. Li, and R. D. Petrasso, "The potential role of electric fields and plasma barodiffusion on the inertial confinement fusion database," Phys. Plasmas **18**(5), 056308 (2011).
[8]C. Bellei, P. A. Amendt, S. C. Wilks, M. G. Haines, D. T. Casey, C. K. Li, R. Petrasso, and D. R. Welch, "Species separation in inertial confinement fusion fuels," Phys. Plasmas **20**(1), 012701 (2013).
[9]K. Molvig, N. M. Hoffman, B. J. Albright, E. M. Nelson, and R. B. Webster, "Knudsen layer reduction of fusion reactivity," Phys. Rev. Lett. **109**, 095001 (2012).
[10]J. D. Jukes, "The structure of a shock wave in a fully ionized gas," J. Fluid Mech. **3**(03), 275–285 (1957).
[11]V. D. Shafranov, "The structure of shock waves in a plasma," Sov. Phys. JETP **5**, 1183 (1957).
[12]Ya. B. Zel'dovich and Yu. P. Raizer, *Physics of Shock Waves and High-Temperature Phenomena* (Dover, Mineola, New York, 2002).
[13]P. A. Amendt, J. L. Milovich, S. C. Wilks, C. K. Li, R. D. Petrasso, and F. H. Sguin, "Electric field and ionization-gradient effects on inertial-confinement-fusion implosions," Plasma Phys. Controlled Fusion **51**(12), 124048 (2009).
[14]D. W. Forslund and C. R. Shonk, "Formation and structure of electrostatic collisionless shocks," Phys. Rev. Lett. **25**, 1699–1702 (1970).
[15]M. Y. Jaffrin and R. F. Probstein, "Structure of a plasma shock wave," Phys. Fluids **7**(10), 1658–1674 (1964).
[16]D. R. Welch, D. V. Rose, C. Thoma, R. E. Clark, C. B. Mostrom, W. A. Stygar, and R. J. Leeper, "Kinetic simulation of thermonuclear-neutron production by a 10^7-A deuterium Z pinch," Phys. Plasmas **17**(7), 072702 (2010).
[17]M. S. Greywall, "Thickness of an embedded ion shock," Phys. Fluids **18**(11), 1439 (1975).
[18]F. Vidal, J. P. Matte, M. Casanova, and O. Larroche, "Ion kinetic simulations of the formation and propagation of a planar collisional shock wave in a plasma," Phys. Fluids B: Plasma Phys. **5**(9), 3182 (1993).
[19]S. I. Braginskii, *Reviews of Plasma Physics* (Consultants Bureau, New York, 1965), Vol. 1.
[20]J. D. Huba, *NRL Plasma Formulary* (Naval Research Laboratory, 2007).
[21]N. A. Krall and A. W. Trivelpiece, *Principles of Plasma Physics* (McGraw-Hill, Inc., 1973).
[22]C. Bellei, P. A. Amendt, S. C. Wilks, D. T. Casey, C. K. Li, R. Petrasso, and D. R. Welch, Phys. Plasmas **20**, 044701 (2013).
[23]O. Larroche, "Ion Fokker-Planck simulation of D^3He gas target implosions," Phys. Plasmas **19**(12), 122706 (2012).
[24]J. T. Larsen and S. M. Lane, "HYADES-A plasma hydrodynamics code for dense plasma studies," J. Quant. Spectrosc. Radiat. Transfer **51**(1–2), 179–186 (1994).
[25]H. Brysk, "Fusion neutron energies and spectra," Plasma Phys. **15**(7), 611 (1973).
[26]H.-S. Bosch and G. M. Hale, "Improved formulas for fusion cross-sections and thermal reactivities," Nucl. Fusion **32**(4), 611 (1992).
[27]S. Atzeni and J. Meyer-Ter-Vehn, *The Physics of Inertial Fusion* (Oxford University Press, 2004).
[28]T. Takizuka and H. Abe, "A binary collision model for plasma simulation with a particle code," J. Comput. Phys. **25**(3), 205–219 (1977).
[29]K. Nanbu, "Theory of cumulative small-angle collisions in plasmas," Phys. Rev. E **55**, 4642–4652 (1997).
[30]P. W. Rambo and R. J. Procassini, "A comparison of kinetic and multifluid simulations of laser-produced colliding plasmas," Phys. Plasmas **2**(8), 3130 (1995).
[31]B. A. Trubnikov, *Particle Iinteraction in a Fully Iionized Plasma in Reviews of Plasma Physics* (Consultants Bureau, New York, 1965), Vol. 1.
[32]B. Appelbe and J. Chittenden, "The production spectrum in fusion plasmas," Plasma Phys. Controlled Fusion **53**(4), 045002 (2011).